Hindawi Publishing Corporation
Journal of Nanomaterials
Volume 2014, Article ID 482372, 6 pages
http://dx.doi.org/10.1155/2014/482372

Research Article

Crystallites of α-Sexithiophene in Bilayer Small Molecule Organic Solar Cells Double Efficiency

Michal Radziwon, André Luis Fernandes Cauduro, Morten Madsen, and Horst-Günter Rubahn

Mads Clausen Institute, University of Southern Denmark, NanoSYD, Alsion 2, 6400 Sønderborg, Denmark

Correspondence should be addressed to Michal Radziwon; michal@radziwon.pl

Received 29 December 2013; Revised 30 March 2014; Accepted 31 March 2014; Published 11 May 2014

Academic Editor: Wen Lei

Recent efforts in research and development of small molecule based organic solar cells have led to power conversion efficiencies exceeding 10%. Understanding the incorporated interfaces in these devices is an utterly important parameter for their improvement. Here we investigate the influence of α-sexithiophene (α-6T) nanostructures on the performance parameters of α-6T/C_{60} inverted bilayer solar cells. By *in situ* controlled growth, crystalline α-6T nanostructures are formed in the devices and a correlation between the morphology of the structures and the device performance is presented. Under certain, well-defined circumstances, we observe an efficiency increase of around 100% when implementing crystalline nanostructures.

1. Introduction

The device performance of small molecule organic solar cells has significantly advanced in recent years and power conversion efficiencies of up to 12% have now been reached [1]. As demonstrated in the past, one of the methods to improve the performance of small molecule devices is through controlled formation of organic nanoscale crystalline structures, as this can lead to both an increased donor-acceptor interface area and an improved intermolecular packing in the donor layer [2, 3], which in turn can lead to both improved charge carrier generation and charge transport properties in the devices. The importance of molecular packing is due to the fact that in conjugated oligomers a strong anisotropy in the charge transport properties is observed, which can be attributed to the anisotropy of the molecules themselves. In the case of α-sexithiophene (α-6T), the herringbone packed monoclinic crystalline system ensures a strong π-π overlap in the planes parallel to the long molecular axes, whereas the overlap in the planes perpendicular to the long molecular axes is small.

In the past, it has been demonstrated that the nanocrystalline morphology in small molecule organic solar cells could be optimized through, for example, thermal [3, 4] or solvent [5] annealing processes as well as by the use of solvent additives [2]. Work on *in situ* controlled growth of crystalline nanostructures from physical vapor deposition through oblique angle deposition [6] has also been demonstrated as a way of improving the performance of small molecule based solar cells. In the present study, we focus on *in situ* controlled growth of α-6T nanoscale crystalline structures for solar cell applications. Previously, it has been shown that structures varying in shape, size, and molecular packing can be obtained from α-6T thin films formed through organic molecular beam deposition (OMBD) on various substrates including mica [7], titanium oxides [8], and gold [9]. We recently demonstrated the growth of α-6T nanoscale structures on C_{60} thin films [10], which, especially from a device point of view, is interesting, as it allows for direct implementation in inverted organic solar cells. The α-6T/fullerene system has previously been investigated in standard configuration solar cells [4] and despite the fact that the power conversion efficiencies of these systems are not higher than 1% for standard configuration devices [4], amongst others from a poor spectral match between their absorption spectra and

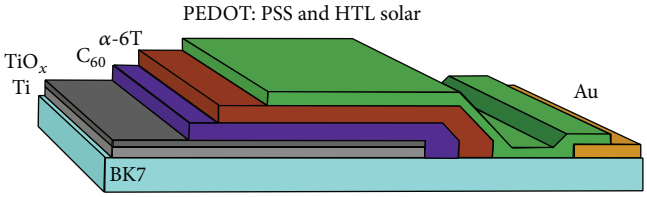

FIGURE 1: Schematic diagram of the inverted α-6T/C_{60} solar cell structure employed in this work.

the solar spectrum, they are still quite interesting as they can serve as a model system [11] for basic research on processes involved in crystalline organic solar cells. Similar studies on crystalline small molecule bilayer devices have recently been carried out on Rubrene/C_{60} systems, which show the importance of controlling the molecular packing in small molecule based organic solar cells [12].

In order to utilize the phenomenon of α-6T nanostructure formation on C_{60} films in organic solar cells, the inverted configuration of the investigated system has been chosen (see Figure 1). The solar cells are fabricated on Ti/TiO_x cathodes using a PEDOT:PSS/HTL solar mixture as an anode. The resulting devices show a clear correlation between the power conversion efficiency and the crystalline structure formation, and a 100% increase in power conversion efficiency is obtained at optimum morphology of the α-6T layers.

2. Materials and Methods

300 μm BK7 glass wafers were precleaned by sonication for 30 s in acetone, rinsed with deionized water, and spindried. A negative photolithography process, followed by e-beam evaporation of a 3 nm Ti adhesive layer and 30 nm of Au, defined the device cathodes and anodes. Then, a shadow mask was introduced to deposit 20 nm of Ti in the cathode regions only, and the wafer was cut into 20 mm × 10.5 mm substrates containing 6 devices each. Prior to deposition of organic layers, the substrates were precleaned by an ultrasonic bath in acetone for 5 min, rinsed with isopropyl alcohol and deionized water, blow-dried with N_2, and exposed to 130 W RF glow discharge oxygen plasma for 90 s. The latter treatment also forms a thin layer of TiO_x on the surface, which has been demonstrated to work as a cathode interfacial layer in organic solar cells [13].

For formation of the active organic layer, 20 nm of commercially available fullerene C_{60} (Sigma-Aldrich, purity 99,5%) was evaporated in an OMBD system, under a deposition pressure of ca.10^{-7} mbar and at a growth rate of 0.3 Å/s. Subsequently, without breaking the vacuum, 30 nm of commercially available α-6T (Tokyo Chemical Industry Co., Ltd.) was evaporated under the same pressure at a growth rate of 0.1-0.2 Å/s at temperatures of the substrate holder ranging between 300 K and 390 K. A shadow mask defined the desired exposure area. A water-cooled, calibrated quartz microbalance was used for *in situ* detection of the nominal thickness and growth rate. Immediately after the deposition, the substrates were moved into a N_2 dry glove box where spin coating of a 1 : 1 mixture of the commercially available conductive polymer HTL SOLAR and CPP PEDOT (Heraeus Precious Metals GmbH & Co. KG) was performed at 1000 RPM for 45 s. The substrates were then annealed for 30 min at 360 K. After 10 min cooldown at room temperature, commercially available UV curable encapsulant (DELO katiobond LPVE) was spun at 4000 RPM for 45 s. A schematic diagram of the device architecture is presented in Figure 1.

The devices were characterized using a Newport 9600 solar simulator with an AM 1.5 G filter set to 1 sun with a Newport 91150-KG1 reference cell. The devices were light-soaked for 15 min prior to measurement. *I-V* curves have been taken with a Keithley 2400 series source meter, by scanning in the 0 mV–500 mV bias range. The V_{OC} value was obtained in a separate measurement, where the source meter was set to source zero current. The reported values are the averages of the measurements across the substrate. Afterwards, epifluorescence micrographs were taken (Nikon Eclipse ME-600, Hg lamp, excitation 465 nm–469 nm, detection 515 nm–555 nm). External quantum efficiency (EQE) measurements were performed by irradiating the samples with a 150 W Xe lamp through a Monochromator (VIS-NIR Newport Cornerstone 1/4 m) followed by fiber coupling into a Mitoyo FS-70 microscope. The external quantum efficiency measurements were carried out in air at 300 K using the same conditions aforementioned. A Si calibrated photodiode (Hamamatsu S2386-44 K) was used to measure the incident power. Reflectance measurements were conducted using a Spectroscopic Ellipsometer (TFProbe Sun Angstrom Technology SE200BA) set 45° with respect to normal incidence.

3. Results and Discussion

In order to investigate the effect from heating the substrates during deposition of α-6T molecules on the morphology of the underlying C_{60} layers, AFM scans of the C_{60} layers directly after deposition and after a postannealing treatment at 420 K were conducted. The RMS roughness from the two different scans is 1.5 nm and 1.6 nm, respectively, which demonstrates that the surface morphology does not change during the heating of the substrates (see Figure 2).

The deposition of α-6T molecules at different substrate temperatures led to the formation of thin films with different morphologies. Epifluorescence micrographs of the α-6T thin films obtained at different substrate temperatures are presented in Figure 3. The micrographs were taken through the UV absorbing encapsulant, which required application of suitable filters in the microscope. At room temperature, a rough continuous film is observed, while at 320 K, small (<3 μm) clusters are formed at individual nucleation points (Figures 3(a) and 3(b)). At 330 K, we observe a mesh of fiber-like structures formed in randomly distributed domains of various sizes, while at 340 K, such structures fully cover the surface area (Figures 3(c) and 3(d)). At an increased substrate temperature of 360 K, the formation of fiber-like structures persists but, contrary to the sample prepared at 340 K, the structures are clearly separated by the areas where

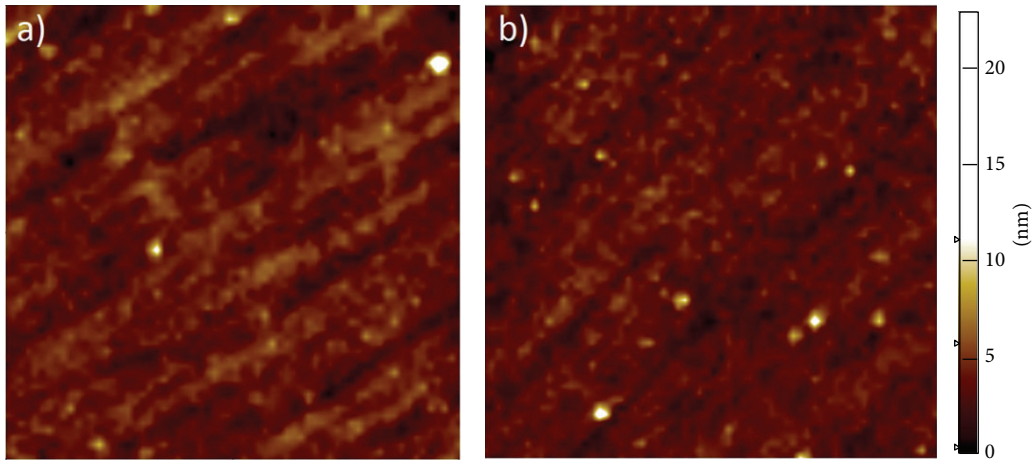

(a) (b)

Figure 2: 25 μm by 25 μm AFM scans of C_{60} as deposited at room temperature (a) and postannealed at 420 K (b).

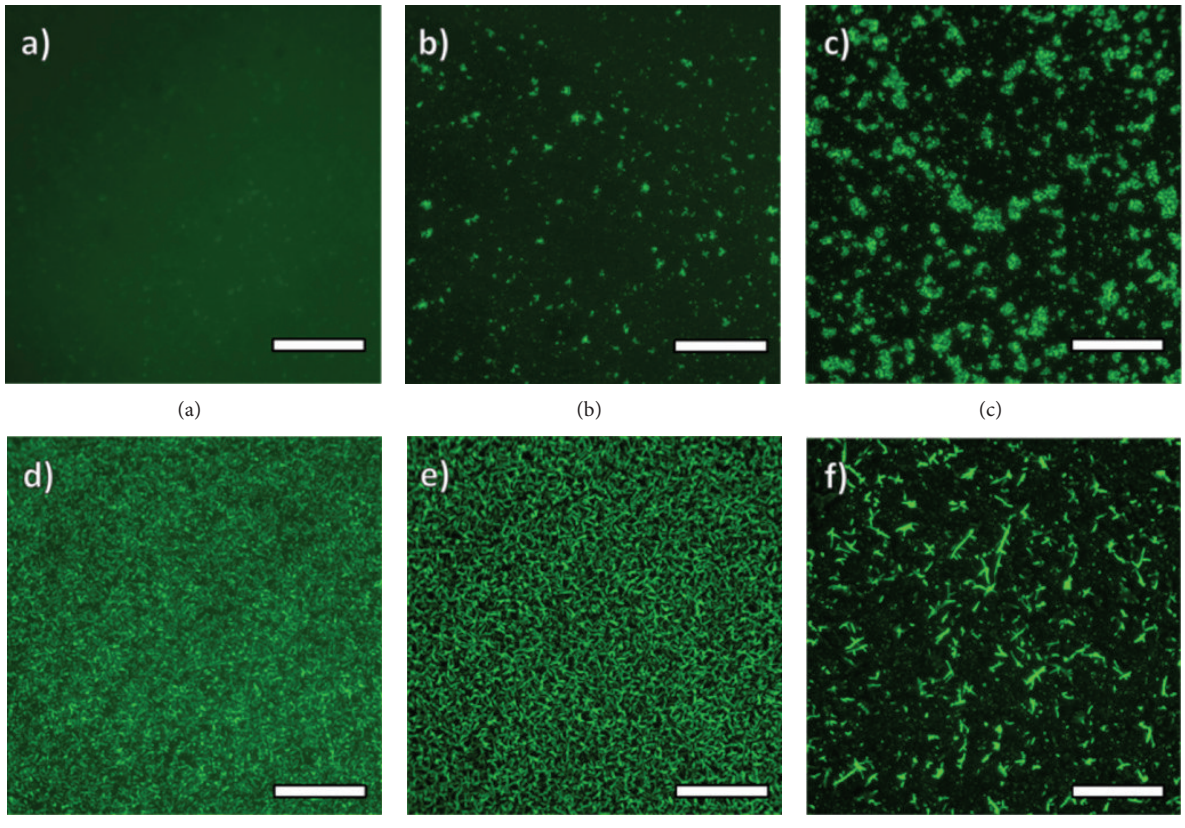

(a) (b) (c)

(d) (e) (f)

Figure 3: Epifluorescence micrographs of α-6T/C_{60} solar cells with electron donor layer deposited at 300 K, 320 K, 330 K, 340 K, 360 K, and 390 K, from (a) to (f), respectively. The scale bars are 20 μm. As the encapsulant layer absorbs UV light, 460 nm–495 nm excitation and 515 nm–555 nm emission filters were employed.

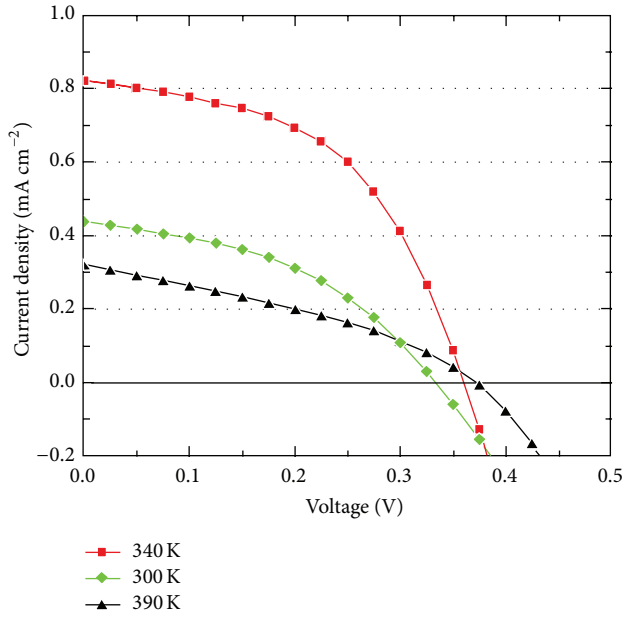

FIGURE 4: J-V curves of organic solar cells fabricated at different substrate temperatures during α-6T.

virtually no fluorescence is observed (Figure 3(e)). At 390 K, 10 μm–20 μm long, straight, and branching fibers are formed, which are surrounded by a mesh of shorter ones –2 μm–5 μm (Figure 3(f)). A similar temperature dependent morphology was observed for thicker (100 nm) α-6T thin films on C_{60} layers, where the crystalline nature was investigated via XRD and fluorescence polarimetry measurements [10]. It could be concluded, that although the films formed at elevated temperatures are dominated mainly by the presence of standing molecules, the formed fiber-like structures consist of lying molecules.

In Figure 4, representative J-V curves from devices consisting of the α-6T layers grown at 300 K, 340 K, and 390 K are shown. At these temperatures, distinct differences in the device performances are obtained, which is related to the morphology of the formed nanostructures. At 330 K–340 K, a mesh of crystalline fibers starts to be formed (Figures 3(c) and 3(d)) along with crystallites consisting of standing molecules. A crystalline structured interface can lead to less trap sites and more efficient exciton dissociation [14], and the lying molecules in fiber-like structures do not only provide areas with preferential orientation of the high mobility axis in the α-6T layer [15, 16] but also facilitate enhanced absorption as the transition dipoles in those are almost perpendicular to the direction of the incident light. The crystallites consisting of standing molecules could also enhance the performance of the devices by facilitating efficient horizontal charge transport from the α-6T nanostructures to the transparent electrode. In combination, these effects should result in an increase of the short circuit current density as well as in a drop of the equivalent series resistance, which can explain the J-V curves for the 340 K devices compared to the 300 K devices. At temperatures higher than 340 K, the surface mobility of the individual α-6T molecules is high enough to cause the material to form separated fibers, which increase in size with the temperature.

In Figure 5, the characteristic device parameters for the solar cells fabricated with different α-6T morphologies are shown. As expected, the open circuit voltage (V_{OC}) shows only little variation with temperature (Figure 5(a)), mostly due to the fact that its value is predominantly determined by the electronic properties of the materials used [17]. The short circuit current density (J_{SC}), fill factor (FF), and power conversion efficiency (PCE) all exhibit a raise in the 330 K–340 K range (Figures 5(b)–5(d)). The PCE shows an increase of about 100% at a substrate temperature of 340 K in comparison to 300 K. At substrate temperatures of 360 K and higher, larger α-6T fibers are being formed and α-6T depleted areas occur, which leads to a decrease of the overall junction area, which explains the eventual drop in the short circuit current density and PCE.

To further elaborate on the efficiency enhancement observed in devices including crystalline structures formed at 340 K, EQE and effective absorption spectra were taken for cells consisting of α-6T layers grown at 300 K and 340 K, respectively (Figure 6). The effective absorption is here defined as "100%-reflection" of the 340 K sample using the 300 K sample as a reference, as this directly relates to their change in absorption. It is evident that the EQE in the 340 K devices is improved over the investigated wavelength range compared to the 300 K devices. The effective absorption also shows that the 340 K devices exhibit stronger light absorption compared to the 300 K samples, due to the formation of the crystalline nanostructures at the elevated temperature. Notably though, as the EQE ratio (ratio between the EQE at 340 K and the EQE at 300 K, not plotted) remains almost constant over the investigated wavelength range, it can be interpreted that the absorption enhancement is not the main factor for the increase in charge collection at short circuit conditions. The improvement is instead considered to take place following absorption of photons in the cell, namely, in the subsequent exciton dissociation process and charge collection at the electrodes, which can be ascribed to the crystalline structure formation in these devices. The crystalline structure formation could lead to improved exciton dissociation, as recently demonstrated in crystalline Rubrene/C_{60} solar cells [12], as well as to improved charge transport properties. Similar morphology dependent improvement in charge collection properties has been demonstrated for postannealed small molecule mixed heterojunction cells [18]. Note, however, that in these cells, due to the presence of a mixed heterojunction, the annealing step leads to a change in both the molecular packing and the domain sizes of the acceptor and donor phases.

4. Conclusions

In this work, we have investigated the influence of various α-6T nanostructures, formed by OMBD at substrate temperatures ranging between 300 K and 390 K, on the performance of inverted organic α-6T/C_{60} solar cells. We have shown that

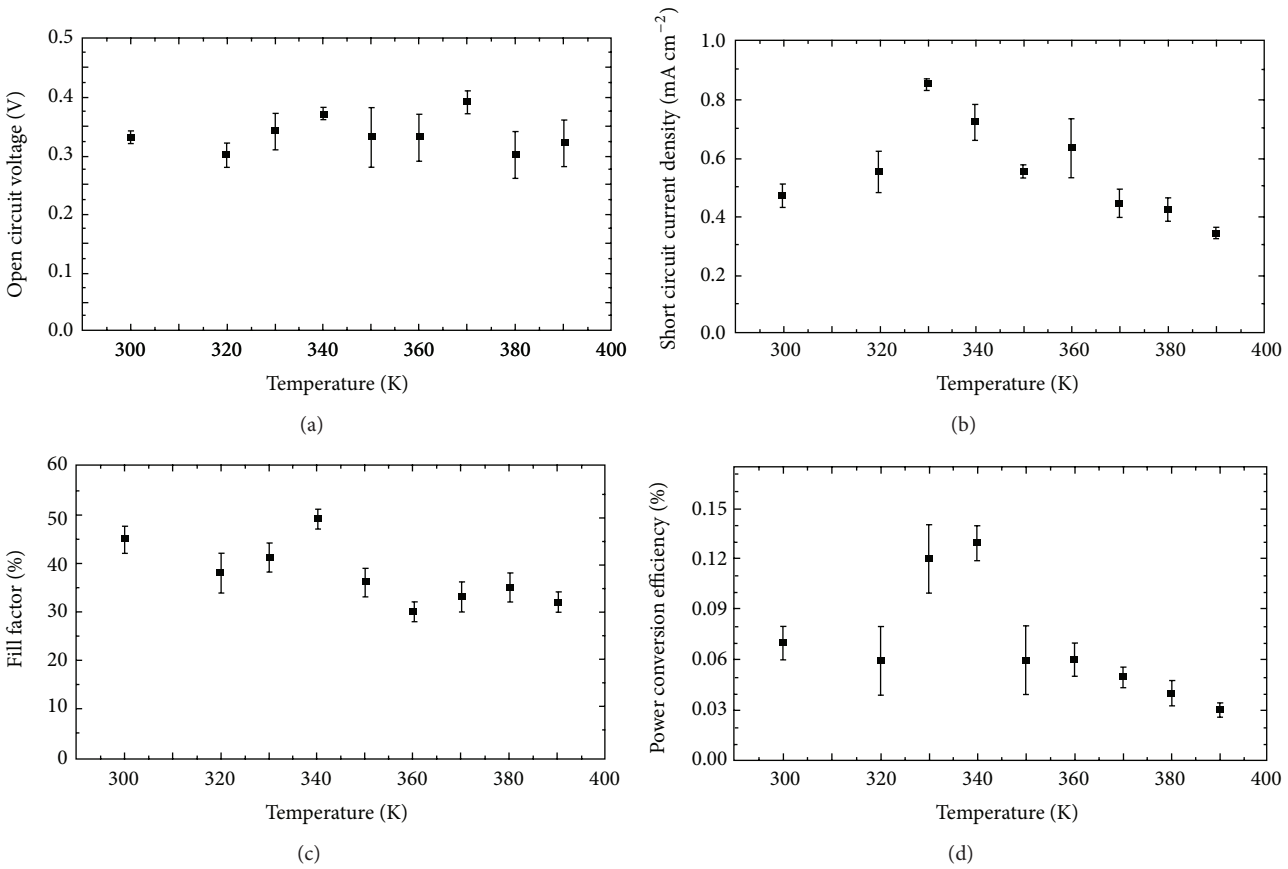

Figure 5: Performance parameters α-6T/C_{60} solar cells with electron donor layer deposited at various surface temperatures.

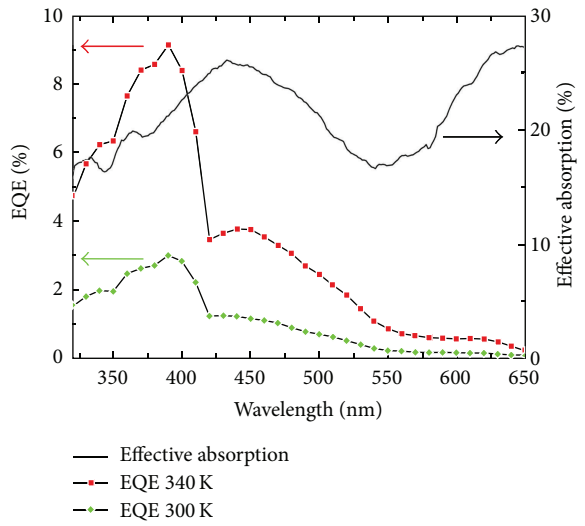

Figure 6: External quantum efficiency and effective absorption extracted from "100%-reflection ratio" of the sample α-6T (@340 K)/C_{60} to α-6T (@300 K)/C_{60}.

controlled growth of nanostructures in the electron donor layer leads to a power conversion efficiency enhancement of around 100% in the 330 K–340 K temperature range. This range is characterized by a maximum density of fiber-like structures which due to their internal molecular packing are responsible for improving both the charge carrier generation and collection at the electrodes. At higher temperatures, the low density of larger fibers leads to a reduced junction area and thus a worse device performance.

Conflict of Interests

The authors declare that they have no conflict of interests regarding the publication of this paper.

Acknowledgments

The authors thank the Fabrikant Mads Clausen trust for the financial support of the research presented in this publication. André Luis Fernandes Cauduro is thankful to the CNPq Brazilian research council for granting a scholarship under process no. 213909/2012-0.

References

[1] Heliatek, "Heliatek consolidates its technology leadership by establishing a new world record for organic solar technology with a cell efficiency of 12%," 2013, http://www.heliatek.com/newscenter/latest_news/.

[2] Y. Sun, G. C. Welch, W. L. Leong, C. J. Takacs, G. C. Bazan, and A. J. Heeger, "Solution-processed small-molecule solar cells with 6.7% efficiency," *Nature Materials*, vol. 11, no. 1, pp. 44–48, 2012.

[3] G. Wei, X. Xiao, S. Wang et al., "Functionalized squaraine donors for nanocrystalline organic photovoltaics," *ACS Nano*, vol. 6, no. 1, pp. 972–978, 2012.

[4] J. Sakai, T. Taima, T. Yamanari, and K. Saito, "Annealing effect in the sexithiophene: C_{70} small molecule bulk heterojunction organic photovoltaic cells," *Solar Energy Materials and Solar Cells*, vol. 93, no. 6-7, pp. 1149–1153, 2009.

[5] G. Wei, S. Wang, K. Sun, M. E. Thompson, and S. R. Forrest, "Solvent-annealed crystalline squaraine: PC70BM (1 : 6) solar cells," *Advanced Energy Materials*, vol. 1, no. 2, pp. 184–187, 2011.

[6] N. Li and S. R. Forrest, "Tilted bulk heterojunction organic photovoltaic cells grown by oblique angle deposition," *Applied Physics Letters*, vol. 95, no. 12, Article ID 123309, 2009.

[7] C. Simbrunner, G. Hernandez-Sosa, M. Oehzelt et al., "Epitaxial growth of sexithiophene on mica surfaces," *Physical Review B: Condensed Matter and Materials Physics*, vol. 83, no. 11, Article ID 115443, 2011.

[8] J. Ivanco, T. Haber, J. R. Krenn, F. P. Netzer, R. Resel, and M. G. Ramsey, "Sexithiophene films on ordered and disordered TiO2(1 1 0) surfaces: Electronic, structural and morphological properties," *Surface Science*, vol. 601, no. 1, pp. 178–187, 2007.

[9] A. J. Mäkinen, J. P. Long, N. J. Watkins, and Z. H. Kafafi, "Sexithiophene adlayer growth on vicinal gold surfaces," *Journal of Physical Chemistry B*, vol. 109, no. 12, pp. 5790–5795, 2005.

[10] M. Radziwon, M. Madsen, F. Balzer, R. Resel, and H. G. Rubahn, "Growth of a-sexithiophene nanostructures on C_{60} thin film layers," *Thin Solid Films*, vol. 558, pp. 165–169, 2014.

[11] S. Veenstra, G. G. Malliaras, H. J. Brouwer et al., "Sexithiophene-C_{60} blends as model systems for photovoltaic devices," *Synthetic Metals*, vol. 84, no. 1, pp. 971–972, 1997.

[12] B. Verreet, P. Heremans, A. Stesmans, and B. P. Rand, "Microcrystalline organic thin-film solar cells," *Advanced Materials*, vol. 25, no. 38, pp. 5504–5507, 2013.

[13] S. Sista, M.-H. Park, Z. Hong et al., "Highly efficient tandem polymer photovoltaic cells," *Advanced Materials*, vol. 22, no. 3, pp. 380–383, 2010.

[14] J. Halls, K. Pichler, R. Friend, S. Moratti, and A. Holmes, "Exciton diffusion and dissociation in a poly (p-phenylenevinylene)/C_{60} heterojunction photovoltaic cell," *Applied Physics Letters*, vol. 68, no. 22, pp. 3120–3122, 1996.

[15] V. Coropceanu, J. Cornil, D. A. da Silva Filho, Y. Olivier, R. Silbey, and J.-L. Brédas, "Charge transport in organic semiconductors," *Chemical Reviews*, vol. 107, no. 4, pp. 926–952, 2007.

[16] J. Y. Lee, S. Roth, and Y. W. Park, "Anisotropic field effect mobility in single crystal pentacene," *Applied Physics Letters*, vol. 88, no. 25, Article ID 252106, 2006.

[17] C. J. Brabec, A. Cravino, D. Meissner et al., "Origin of the open circuit voltage of plastic solar cells," *Advanced Functional Materials*, vol. 11, no. 5, pp. 374–380, 2001.

[18] D. Wynands, M. Levichkova, M. Riede et al., "Correlation between morphology and performance of low bandgap oligothiophene: C_{60} mixed heterojunctions in organic solar cells," *Journal of Applied Physics*, vol. 107, no. 1, Article ID 014517, 2010.